evaluation of cardiac risk before elective vascular surgery. *J Am Coll Cardiol* 1987;9:269–276.
33. Younis LT, Byers S, Shaw L, Barth G, Goodgold H, Chaitman BR. Prognostic value of intravenous dipyridamole thallium scintigraphy after an acute myocardial ischemic event. *Am J Cardiol* 1989;64:161–166.
34. Hendel RC, Layden JJ, Leppo JA. Prognostic value of dipyridamole thallium scintigraphy for evaluation of ischemic heart disease. *J Am Coll Cardiol* 1990;15: 109–116.
35. Brown KA. Prognostic value of thallium-201 myocardial perfusion imaging. *Circulation* 1991;83:363–381.
36. Chouraqui P, Rodriques EA, Berman DS, Maddahi J. Significance of dipyridamole-induced transient dilation of the left ventricle during thallium-201 scintigraphy in suspected coronary artery disease. *Am J Cardiol* 1990;66:689–694.
37. Stratton JR, Speck SM, Caldwell JH, et al. Relation of global and regional left ventricular function to tomographic thallium-201 myocardial perfusion in patients with prior myocardial infarction. *J Am Coll Cardiol* 1988;12:71–77.
38. Younis LT, Byers S, Shaw L, Barth G, Goodgold H, Chaitman BR. Prognostic importance of silent myocardial ischemia detected by intravenous dipyridamole thallium myocardial imaging in asymptomatic patients with coronary artery disease. *J Am Coll Cardiol* 1989;14:1635–1641.
39. Iskandrian AS, Chae SC, Heo J, et al. Independent and incremental prognostic value of exercise single-photon emission computed tomographic thallium imaging in coronary artery disease. *J Am Coll Cardiol* 1993;22:665–670.
40. Ilmer B, Reijs AE, Fioretti P, Reiber JH. Comparative study of three different approaches on the estimation of the lung-heart ratio in thallium-201 scintigrams in relation to the extent of coronary artery disease and left ventricular function. *Eur J Nucl Med* 1991;18:252–258.
41. Mannting F. A new method of quantification of pulmonary thallium uptake in myocardial SPECT studies. *Eur J Nucl Med* 1990;16:213–222.

Generator-Produced Copper-62-PTSM as a Myocardial PET Perfusion Tracer Compared with Nitrogen-13-Ammonia

Eiji Tadamura, Nagara Tamaki, Hidehiko Okazawa, Yasuhisa Fujibayashi, Takashi Kudoh, Yoshiharu Yonekura, Yasuhiro Magata, Ryuji Nohara, Shigetake Sasayama and Junji Konishi

Department of Nuclear Medicine, Third Division, Department of Internal Medicine, Kyoto University Faculty of Medicine, Kyoto, Japan

The purpose of this study was to determine the suitability of ^{62}Cu-pyruvaldehyde bis(N^4-methylthiosemicarbazone) (^{62}Cu-PTSM) for estimating myocardial blood flow (MBF) over a wide range of flow by comparison with ^{13}N-ammonia ($^{13}NH_3$). **Methods:** PET studies using ^{62}Cu-PTSM and $^{13}NH_3$ were performed at rest and after pharmacological vasodilatation in 9 normal subjects and 13 patients with coronary artery disease (CAD). According to the microsphere method, values for the product of the extraction fraction and MBF (ExMBF) were calculated using both tracers. In static images, the percent uptake (normalized to the peak count) of each tracer was measured in patients with CAD. **Results:** The myocardial tracer distribution in the normal subjects was significantly higher in the inferior wall in the ^{62}Cu-PTSM studies and lower in the lateral wall in the $^{13}NH_3$ studies. The ExMBF values showed linear correlation for both tracers in a low flow range. In a high flow range, however, the ExMBF values for ^{62}Cu-PTSM were nonlinearly proportional to the increase of those for $^{13}NH_3$ ($y = 1.1x-0.21x^2$, $r = 0.81$). The percent uptake for both tracers at baseline well correlated linearly ($y = 10.4 + 0.88x$, $R = 0.91$). After pharmacological vasodilatation underestimation of blood flow with ^{62}Cu-PTSM was noted compared to that with $^{13}NH_3$ at high flows ($y = 31.8 + 0.63x$, $r = 0.76$). **Conclusion:** These results suggest that the MBF estimates using ^{62}Cu-PTSM in a low flow range may be as accurate as those with $^{13}NH_3$. In a high flow range, however, the extraction fraction of ^{62}Cu-PTSM is considered to be lower than that of $^{13}NH_3$, and this may limit the estimation of MBF with ^{62}Cu-PTSM after pharmacological vasodilatation.

Key Words: PET; myocardial blood flow; copper-62-PTSM; nitrogen-13-ammonia

J Nucl Med 1996; 37:729–735

Received Apr. 11, 1995; revision accepted Aug. 16, 1995.

For correspondence or reprints contact: Eiji Tadamura, MD, Department of Nuclear Medicine, Kyoto University Faculty of Medicine, Shogoin, Sakyo-ku, Kyoto, 606-01 Japan.

Noninvasive evaluation of myocardial blood flow (MBF) is one of the most important aspects in cardiology. MBF can be quantitatively assessed by: PET using ^{13}N-ammonia ($^{13}NH_3$) (*1–5*) or ^{15}O-water (*6–8*) produced by cyclotron, and ^{82}Rb-chloride (*9*) produced by a generator.

Positron-emitting radionuclides produced by a generator could potentially expand the application of PET to centers that do not have an in-house cyclotron. Several studies have shown that ^{82}Rb, in combination with pharmacologic stress, enables the accurate detection of coronary artery disease (CAD) (*10–12*). PET imaging with ^{82}Rb have relatively low intrinsic resolution because ^{82}Rb emits a high-energy positron that travels a long distance before colliding with an electron to produce two gamma photons (*13*). In addition, generation of ^{82}Sr requires a high-energy cyclotron, which makes this generator expensive. Therefore, alternative generator-produced radiopharmaceuticals for PET have long been desired. The ^{62}Zn/^{62}Cu radionuclide generator is a potential source of radiopharmaceuticals for PET. Copper-62-pyruvaldehyde bis(N^4-methylthiosemicarbazone) (^{62}Cu-PTSM) has been introduced as a new generator-produced perfusion tracer.

Previous investigations suggested that ^{62}Cu-PTSM represented a promising radiopharmaceutical for the evaluation of myocardial perfusion in animals and when applied to the normal human heart (*14–22*). This study was designed to determine the suitability of ^{62}Cu-PTSM for evaluating MBF in patients with CAD as well as in normal subjects over a wide range of flow by comparison with $^{13}NH_3$ (*23*).

MATERIALS AND METHODS

Tracer Preparation

Zinc-62 was obtained by ^{63}Cu(p,2n)^{62}Zn nuclear reaction using natural copper (^{63}Cu, 69.2%) as a target material. A ^{62}Zn/^{62}Cu generator was prepared with $^{62}ZnCl_2$ aqueous solution (1.1GBq, pH 5.0) by the method as previously reported (*24*). In this

TABLE 1
Clinical Data of 22 Subjects

Subject no.	Age (yr)	Sex	Clinical diagnosis	Stenosis on CAD			Study state	
				RCA (%)	LAD (%)	LCX (%)	Rest	Dip
1	34	M	Normal				+	+
2	39	M	Normal				+	+
3	43	M	Normal				+	+
4	49	M	Normal				+	
5	50	M	Normal					+
6	52	M	Normal				+	
7	57	M	Normal					+
8	64	M	Normal					+
9	71	M	Normal				+	
10	68	F	AP	75				+
11	69	F	AP	75			+	+
12	70	M	AP	75	90			+
13	71	F	AP	90	75	75	+	
14	79	M	AP		99	100	+	
15	62	M	inf MI	100	75	100		+
16	62	M	ant MI		99		+	
17	63	M	ant MI		99	90	+	+
18	67	M	ant MI		100		+	
19	68	M	ant MI		100		+	
20	73	M	ant MI		99		+	
21	78	F	ant MI	100	90	75	+	+
22	81	M	lat MI			99		+

MI = myocardial infarction; AP = angina pectoris; ant = anterior; inf = inferior; lat = lateral; RCA = right coronary artery; LAD = left anterior descendence; LCX = left circumflex artery; dip = dipyridamole.

generator system, cation-exchange resin was packed into a column, and ^{62}Zn solution (1.1 GBq, in 2 ml of water, pH 5.0) was loaded to adsorb ^{62}Zn. A glycine solution (200 m*M*) was used as the eluant and ^{62}Cu-glycine complex was obtained in glycine solution. PTSM was prepared as described previously (*25*). The ^{62}Cu-PTSM was quantitatively obtained by simple mixing of the generator eluate, ^{62}Cu-glycine and PTSM solution for a few seconds by a ligand-exchange reaction (*26*). After preparation of the generator, eluate could be acquired at the interval of every 40 to 60 min. The elution efficiency was 60% to 70%, and the radiochemical purity was greater than 95%. The product was acquired in a total volume of 4 ml of ^{62}Cu-PTSM (0.1 m*M* PTSM in 5% dimethyl sulfoxide) with glycine solution.

Nitrogen-13-ammonia was produced by $^{16}O(p,\alpha)^{13}N$ nuclear reaction with water irradiation using an ultracompact cyclotron followed by reduction to ^{13}N-ammonia with titanous hydroxide. The ^{13}N-ammonia was collected in saline solution and passed through a Millipore filter (*27–29*).

Subjects

The study group consisted of 22 subjects (18 males and 4 females; age 62.3 ± 12.9 yr, mean ± s.d.) including 13 patients with angiographically confirmed ischemic heart disease and 9 healthy male volunteers (Table 1). None of the volunteers had a history of cardiac diseases, hypertension or any cardiac symptoms. Each subject gave a written informed consent approved by the Ethical Committee of Kyoto University Faculty of Medicine.

PET

The PET studies were performed using a whole-body PET camera. It provides 15 slices at 7 mm intervals simultaneously. The scanner has an effective resolution of 9 mm and an axial resolution of 7 mm at full width half maximum after reconstruction (*30*). Each subject was positioned on the PET camera with an aid of ultrasound technique. At the beginning of the PET study, a transmission scan was obtained for 20 min using a ^{68}Ge/^{68}Ga source external to the patient in order to correct photon attenuation.

PET cardiac imaging using ^{62}Cu-PTSM (421 ± 76 MBq) and $^{13}NH_3$ (411 ± 82 MBq) were performed with the same dynamic acquisition protocol. Serial images were recorded for 10 min immediately after intravenous administration of each tracer as a slow bolus over 30 sec. The acquisition sequence consisted of 12 × 10-sec images and 8 × 60–sec images. In addition, the last set of eight contiguous images (2–10 min after tracer administration) served as static images. Following reconstruction of 15 transverse tomograms, oblique tomograms parallel to the long- and short-axis of the left ventricle were also reformatted. Fifteen subjects (six normal subjects and nine patients with CAD) in this study group underwent both $^{13}NH_3$ and ^{62}Cu-PTSM studies at baseline. Thirteen subjects (six normal subjects and seven patients with CAD) were examined with both tracers after dipyridamole infusion (0.56 mg/kg body weight during 4 min) in order to assess regional myocardial blood flow during hyperemic condition. Heart rate, blood pressure and 12-lead electrocardiogram (ECG) were recorded before and every 1 min during the protocol. All subjects who underwent dipyridamole studies had abstained from caffeine for 24 hr. In each subject, these studies were performed within 2 days and appropriate time delays to allow for decay of tracers were interspersed between the different PET studies.

Data Analysis

The regional myocardial distribution of each tracer in normal subjects was evaluated at rest and after pharmacological vasodilatation. The circumferential profile curve was generated from apical to basal short-axis slices to create a polar map of 100% as a maximum count in each ^{62}Cu-PTSM and $^{13}NH_3$ distribution. To assess the heterogeneity of the tracer distribution the left ventricular myocardium was subsequently divided into four major segments (anterior, lateral, inferior, septal) on the polar map, and the

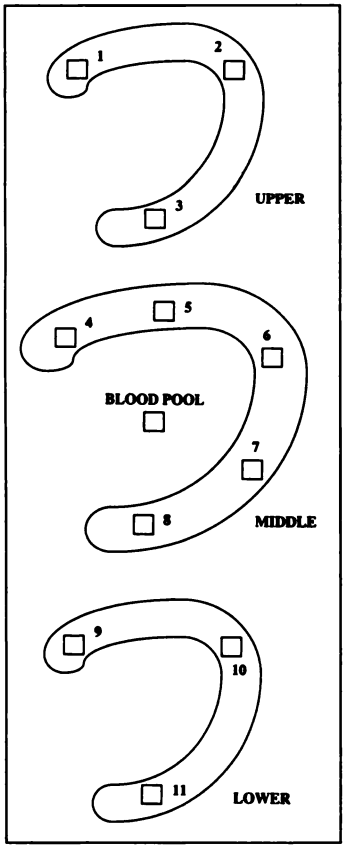

FIGURE 1. Three transaxial slices illustrate 11 ROI definition. Small ROI assigned to the left ventricular blood pool to derive arterial input functions is also illustrated.

regional data were expressed as the mean percent of the maximum myocardial activity ± s.d. for each study.

In order to compare the image quality of each tracer, regions of interest (ROIs) were placed over the liver and left ventricular cavity on the static images. The count ratios of myocardium-to-blood pool and myocardium-to-liver were calculated in each study.

Figure 1 shows 11 ROIs placed over the left ventricular myocardium on the static images. The myocardial uptake percent in static images was calculated after the normalization to each peak value in the study. In addition, maximum-to-minimum count ratio in each study of patients with CAD was also calculated to determine the contrast between ischemic and normal segments.

Since ^{62}Cu-PTSM shows markedly prolonged myocardial retention and rapid blood-pool clearance (*17,19*) and $^{13}NH_3$ also exhibits properties that resemble those of microspheres (*31*), the microsphere method (*32*) was applied for quantitative analysis of MBF. According to this method, MBF is expressed as follows:

$$\text{ExMBF} = \frac{C_T(t)}{\int_0^t C_a(\tau)d\tau}, \qquad \text{Eq. 1}$$

where E is the extraction fraction of each tracer, $C_T(t)$ represents tissue radioactivity and Ca(t) is the arterial input function obtained from the ROIs drawn on the left ventricular cavity after correction for blood metabolites. In order to acquire the blood-pool activities, two ROIs were drawn on the cavity of the mid-ventricular imaging planes and were averaged for reduction of the noise level. Then these ROIs and the 11 ROIs placed over the myocardium described above were copied on serial dynamic PET images in each study. The blood pool in the ^{62}Cu-PTSM and $^{13}NH_3$ studies includes metabolites. Therefore, in order to correct for metabolites in the ^{62}Cu-PTSM studies, the octanol-extractable part of ^{62}Cu was considered as the corrected arterial input function (*33*). We used the mean ratio of radioactivity in the octanol phase to the total blood activity obtained from the arterial blood samples in ten other subjects. A monoexponential curve was fitted to the percent of octanol-extractable ^{62}Cu-PTSM in blood over time. The ratio (y) at time t (sec) was expressed as follows: $y = 0.921 \times \exp(-0.00614t)$ ($R = 0.945$) (*34*). Blood-pool activities of $^{13}NH_3$ were corrected according to a previous investigation (*35*). At 120 sec after injection of each tracer, ExMBF was calculated according to Equation 1.

Statistical Analysis

All data are expressed as mean ± s.d. Blood pressure, heart rate, count ratios of different organs and those of normal-to-ischemic segments in ^{62}Cu-PTSM and $^{13}NH_3$ studies were compared by paired Student's t-test. Hemodynamic data after dipyridamole infusion were compared with those at baseline by unpaired Student's t-test. The regional myocardial tracer distribution in myocardial segments on the bull's eye map was compared by analysis of variance with the Fisher's protected least significant difference method. Probability values <0.05 were considered significant. Regression equations were calculated by the least-squares fit to first- or second-order polynominal functions.

RESULTS

Hemodynamic and Symptomatic Responses to Dipyridamole

Sixteen subjects were studied with both ^{62}Cu-PTSM and $^{13}NH_3$ at rest. The mean systolic blood pressure and heart rate was 129 ± 23 mmHg and 67 ± 8 bpm, respectively. Thirteen subjects were studied with each tracer after dipyridamole infusion and their systolic blood pressure and heart rate was 126 ± 32 mmHg (p = n.s.) and 80 ± 14 bpm ($p < 0.001$), respectively. Hemodynamic parameters did not differ significantly between ^{62}Cu-PTSM and $^{13}NH_3$ studies.

There were no serious side effects during dipyridamole infusion. One patient needed intravenous administration of aminophylline because of epigastric pain at the time of ^{62}Cu-PTSM study. Aminophylline was infused 5 min after tracer administration and would not have affected the result of this study because the input into the myocardium was almost completed within 2 min. Some mild symptoms of flushing, headache, chest pains and dizziness were observed in nine subjects, but these subsided promptly without treatment.

Image Quality and Regional Tracer Distribution in Normal Subjects

Figure 2 shows images of the heart of a normal subject obtained with ^{62}Cu-PTSM and $^{13}NH_3$ at rest and after dipyridamole infusion. Excellent image quality of the myocardium was observed with both tracers, although $^{13}NH_3$ provided superior image quality because of its high contrast between myocardium and underlying liver tissue or blood pool. Table 2 shows the mean count ratios of myocardium to blood and myocardium to liver in static images at rest and after pharmacological vasodilatation. At baseline, myocardium to blood count ratio was higher with $^{13}NH_3$ than with ^{62}Cu-PTSM (5.21 ± 1.61 versus 3.13 ± 0.56, respectively, $p < 0.001$) and the myocardium to liver count ratio was also higher with $^{13}NH_3$ (1.20 ± 0.31 versus 0.67 ± 0.23, respectively, $p < 0.001$). Similar differences were observed after pharmacological vasodilatation (Table 2).

Figure 3 shows the regional myocardial distribution of ^{62}Cu-PTSM and $^{13}NH_3$ at rest and after dipyridamole infusion in six normal subjects. The ^{62}Cu-PTSM uptake was significantly greater in the inferior region as compared to the lateral and septal regions at rest and to the anterior, lateral and septal regions after pharmacological vasodilatation. The $^{13}NH_3$ uptake was significantly lower in the lateral region of the myocardium

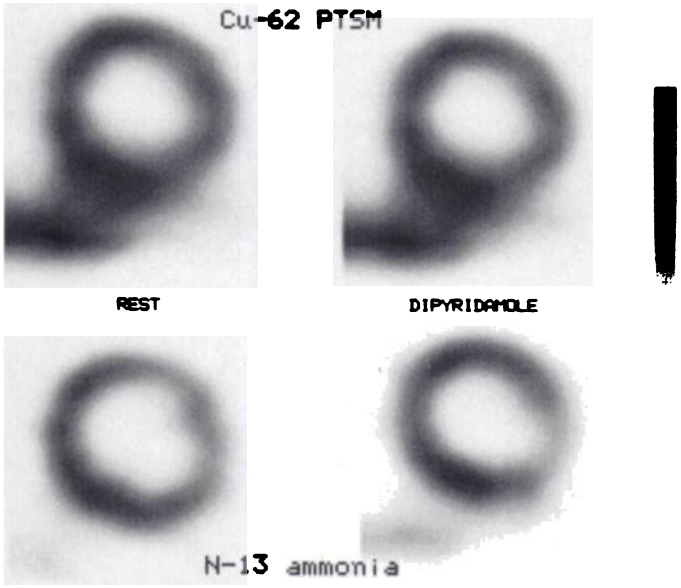

FIGURE 2. Example of ^{62}Cu-PTSM (top) and $^{13}NH_3$ (bottom) studies in a normal subject in the short-axis view at baseline (left) and after pharmacological vasodilatation (right). Good image quality of the heart is observed with both tracers. Note the high liver activities adjacent to the inferior wall in ^{62}Cu-PTSM studies and decreased tracer uptake in the lateral wall in ^{13}N-ammonia studies.

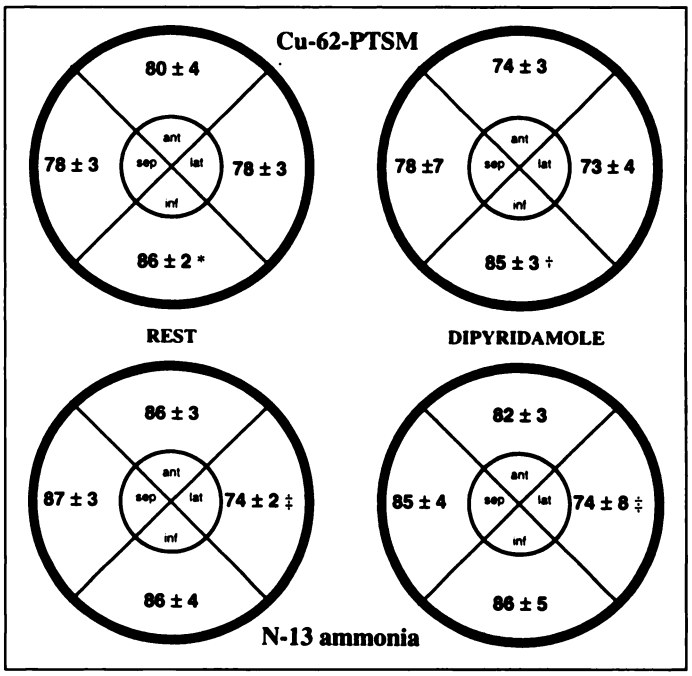

FIGURE 3. Polar map display of myocardial tracer distribution of six normal subjects at rest and after pharmacological vasodilatation. Mean regional myocardial ^{62}Cu-PTSM and ^{13}N-ammonia distribution is expressed as a percent of maximal activity for each study. Each myocardium is divided into four regions: anterior (ant), lateral (lat), septal (sep), inferior (inf) regions. *$p < 0.05$ versus lateral and septum. †$p < 0.05$ versus anterior, lateral and septum. ‡$p < 0.05$ versus anterior, septal and lateral regions.

as compared to the anterior, septal and inferior regions both at rest and after pharmacological vasodilatation.

Relative Tracer Distribution in Patients with CAD

Figure 4 shows the relationship of the percent uptake of the two tracers at rest and after dipyridamole infusion in patients with CAD. Excellent correlation was observed at rest ($y = 10.4 + 0.88x$, $R = 0.91$). Accordingly, the tracer distributions in the myocardium at rest also showed close correlation with each other (Fig. 5).

After pharmacological vasodilatation, however, some underestimation of high flow segments was noted with ^{62}Cu-PTSM ($y = 31.8 + 0.63x$, $R = 0.76$).

At rest maximum-to-minimum count ratio was 2.72 ± 1.80 in $^{13}NH_3$ studies and 2.43 ± 1.43 in ^{62}Cu-PTSM ones (p = n.s.). After dipyridamole infusion, however, it was 2.50 ± 1.07 and 1.78 ± 0.46, respectively ($p < 0.05$). Thus, the defect contrast after pharmacological vasodilatation was less prominent by ^{62}Cu-PTSM than $^{13}NH_3$ (Fig. 6).

Quantitative Analysis

Figure 7 shows the relationship between the values for ExMBF for the two tracers at rest (n = 15; filled circles) and after pharmacological vasodilatation (n = 13; open circles). The ExMBF values for ^{62}Cu-PTSM correlated in a linear fashion with those for $^{13}NH_3$ in a lower flow range but they were lower with relatively large variation in a high flow range compared to those for $^{13}NH_3$ ($y = 1.1x - 0.21x^2$, $R = 0.81$).

TABLE 2
Count Ratios

	Myocardium-to-Blood	Myocardium-to-Liver
Copper-62-PTSM		
Rest	3.13 ± 0.56*	0.67 ± 0.23‡
Dipyridamole	3.26 ± 0.84†	0.80 ± 0.22§
Nitrogen-13-ammonia		
Rest	5.21 ± 1.61*	1.20 ± 0.31‡
Dipyridamole	5.91 ± 1.99†	1.48 ± 0.38§

*$p < 0.001$; †$p < 0.001$; ‡$p < 0.001$; §$p < 0.001$.

DISCUSSION

These results indicate that ^{62}Cu-PTSM permits estimation of MBF as accurately as $^{13}NH_3$ in patients with CAD as well as normal subjects at rest. After pharmacological vasodilatation, however, the ExMBF values obtained with ^{62}Cu-PTSM were significantly lower with large variation compared to those with $^{13}NH_3$ probably due to the lower extraction fraction in a high flow range.

Copper-62-PTSM was introduced as a new generator-produced perfusion tracer. Previous investigations suggested that ^{62}Cu-PTSM represented a promising radiopharmaceutical for the evaluation of MBF in animals (*15–19*). In addition, Beanlands et al. demonstrated that the time-activity curves of ^{62}Cu-PTSM bear a striking resemblance to those of $^{13}NH_3$ in that both have prolonged tissue retention, and they also reported that good image quality was observed at rest and after pharmacological vasodilatation in six normal human volunteers (*20*). Herrero et al. showed that quantification of MBF was feasible at rest in human volunteers (*21*). They have shown that ^{62}Cu-PTSM is promising for the evaluation of MBF in the human heart.

In our studies, ^{62}Cu-PTSM was also found to provide myocardial perfusion images with good image quality. The image quality, however, was less satisfactory than that obtained using $^{13}NH_3$ because of the lower myocardium-to-blood and myocardium-to-liver contrast as shown in Table 2.

In terms of tracer distribution in normal subjects, our data were consistent with those of previous investigations. There was slightly increased radioactivity in the inferior wall relative to the other myocardial segments in the ^{62}Cu-PTSM studies (*20,22*). This high radioactivity in the inferior wall was thought to be due to the cross contamination of high radioactivity in the

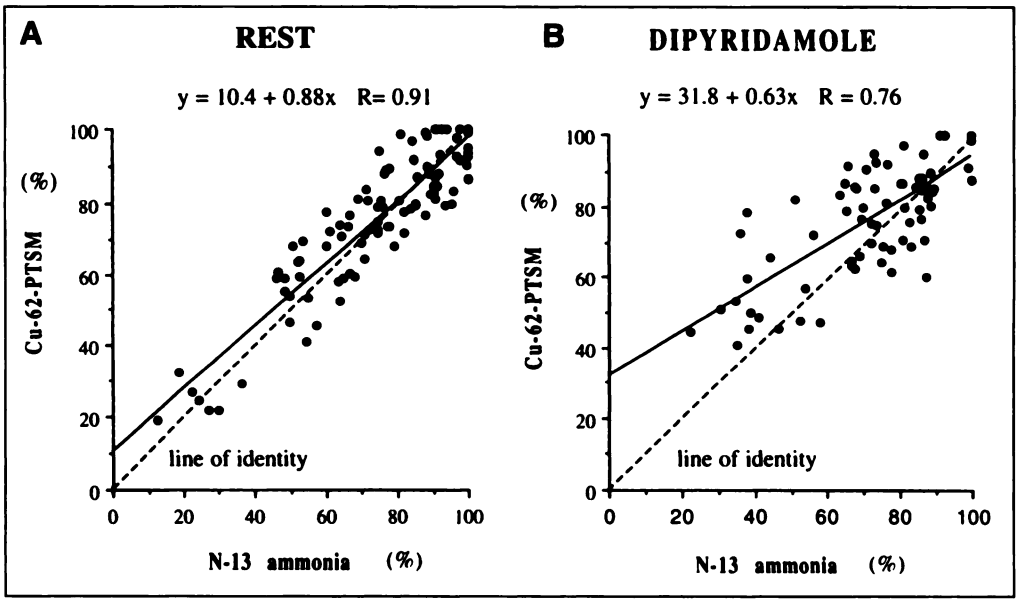

FIGURE 4. Comparison of the percent uptake of each tracer at rest (A) and after dipyridamole infusion (B) in patients with CAD. The linear regression lines and correlation coefficients for the percent uptake are y = 10.4 + 0.88x, R = 0.91 (A), y = 31.8 + 0.63x, R = 0.76 (B).

liver. The $^{13}NH_3$ distribution was also inhomogenous and the low uptake of $^{13}NH_3$ in the lateral wall was observed both at rest and after pharmacological vasodilatation as was also previously reported (*36–38*). Although its mechanism is still unknown, there appears to be a regional metabolic alteration in $^{13}NH_3$ tissue retention (*37*).

Copper-62-PTSM bears a resemblance of $^{13}NH_3$ in that both tracers exhibit properties similar to those of microspheres (*17,19,31*). Both tracers have prolonged tissue retention and rapid clearance from the blood-pool. Therefore the microsphere model was applied for estimation of MBF. As is the case for all extractable perfusion tracers, the myocardial uptake of $^{13}NH_3$ is inversely and nonlinearly proportional to flow (*31*). Thus, in a high flow range, proportionally less tracer is extracted by the myocardium. Shelton et al. demonstrated that the extraction fraction of ^{62}Cu-PTSM plateaued at flow rates greater than 2.5 ml/g/min in dogs (*19*).

Estimation of the accurate input function is essential in order to obtain quantitative values of MBF in the microsphere model. Herrero et al. presented the octanol-extractable part of ^{62}Cu as the corrected arterial input function in five dogs (*21*). We employed here the mean ratio of radioactivity in the octanol phase to the total blood activity obtained from the arterial blood samples in ten other subjects in order to correct for metabolites in the blood pool in the ^{62}Cu-PTSM studies (*34*).

In the quantitative analysis, values of the ExMBF product were calculated for each tracer according to the microsphere method. Bellina et al. (*4*) applied and validated a similar method for quantification of MBF in $^{13}NH_3$ PET studies. While they obtained the input function by gamma variate fitting before integration, we acquired it after correction for metabolites according to the previous investigation (*35*). When the extraction fraction of both tracers is assumed to be equal, ExMBF should also be equal. In this study the ExMBF of ^{62}Cu-PTSM was well correlated in a linear fashion with that of $^{13}NH_3$ in a low flow range as shown in Figure 7. The ExMBF of ^{62}Cu-PTSM, however, showed less marked increase compared

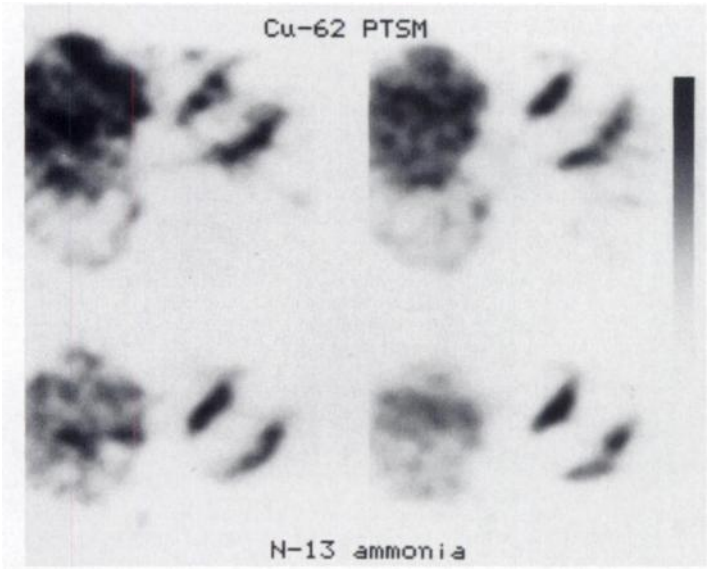

FIGURE 5. Copper-62-PTSM (top) and ^{13}N-ammonia (bottom) contiguous transaxial images obtained at baseline in a patient with anterior myocardial infarction. The tracer distribution in the myocardium correlates closely with each other. Note the high liver activity in ^{62}Cu-PTSM study compared to ^{13}N-ammonia study.

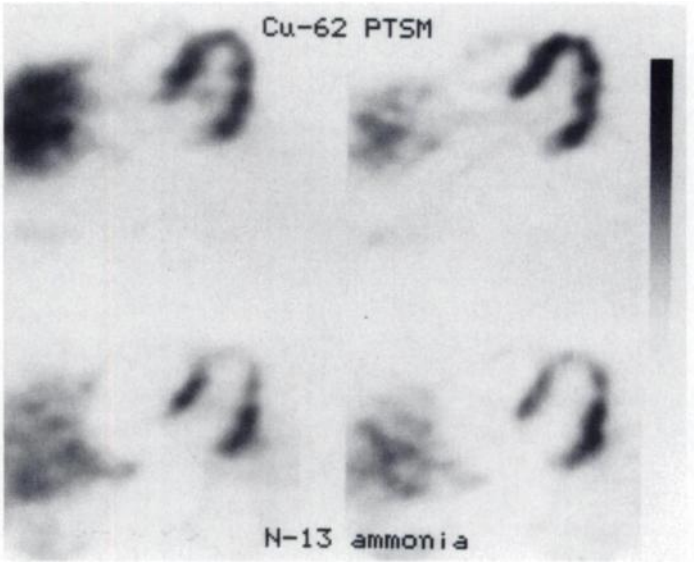

FIGURE 6. Copper-62-PTSM (top) and ^{13}N-ammonia (bottom) contiguous transaxial images of a patient with CAD following dipyridamole infusion. Coronary angiography showed 75%–90% stenosis in the right and left anterior descending coronary artery in this patient. Note that the dipyridamole-induced perfusion defect in the anteroseptal region was more prominent with ^{13}N-ammonia than with ^{62}Cu-PTSM.

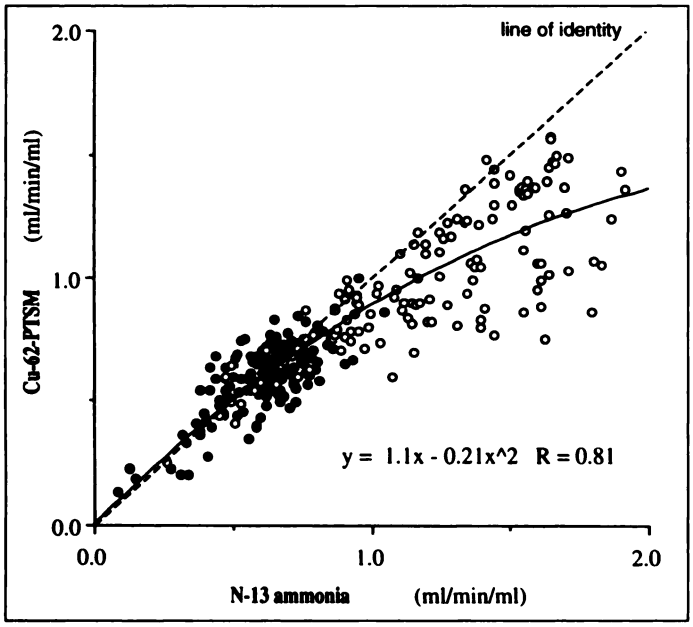

FIGURE 7. Comparison of the ExMBF values between each tracer of 16 subjects at rest (filled circles) and 13 subjects after pharmacological vasodilatation (open circles). The ExMBF values of ^{62}Cu-PTSM increase more gradually according to higher flow than ^{13}N-ammonia.

to that of $^{13}NH_3$ in a high flow range. This result indicates the extraction fraction of ^{62}Cu-PTSM is not as high as that of $^{13}NH_3$ especially in a high flow range. In this respect ^{62}Cu-PTSM may not be suitable for the accurate estimation of hyperemic flow after vasodilatation in the human heart compared to $^{13}NH_3$.

These data also account for the results of relative distribution of each tracer in the patients with CAD. At baseline, the uptake of both tracers was highly correlated because their extraction fractions did not differ in a low flow range. After pharmacological vasodilatation, however, the percent uptake was underestimated with ^{62}Cu-PTSM at high flows. This indicates that the contrast between normal and ischemic segments was less prominent due to the lower extraction fraction of ^{62}Cu-PTSM relative to that of $^{13}NH_3$ in a high flow range. Therefore, ^{62}Cu-PTSM images are unlikely to detect mild coronary artery stenosis. In fact, the dipyridamole-induced perfusion defect in the anteroseptal region observed with $^{13}NH_3$ was not so evident with ^{62}Cu-PTSM (Fig. 6). Further evaluation is needed to determine the feasibility of MBF estimates in a high flow range.

In the quantitative study, ExMBF showed good correlation for the two tracers in a low flow range. Therefore, MBF estimates with ^{62}Cu-PTSM at rest are considered to be as accurate as those with $^{13}NH_3$ in patients with CAD as well as normal subjects. In this respect, clinical application of myocardial tissue viability may be feasible with combined imaging of ^{62}Cu-PTSM and FDG at rest (*39,40*). On the other hand, the MBF estimates obtained with ^{62}Cu-PTSM in a high flow range were significantly underestimated compared to those with $^{13}NH_3$. In this respect, the quantitative estimation of MBF after pharmacological vasodilatation seems to be limited.

Limitations

In this study, MBF estimates by ^{62}Cu-PTSM was compared with those by $^{13}NH_3$ at rest and after pharmacological vasodilatation on different days. Therefore, the MBF may not be absolutely the same in the two ^{62}Cu-PTSM and $^{13}NH_3$ studies especially after pharmacological vasodilatation. Hemodynamic data and frequency of subjective symptoms, however, were not significantly different between these studies.

In this study the microsphere method was applied for obtaining quantitative values of MBF. In this model spillover from the blood pool to the myocardium is not taken into consideration (*5*). In this respect, a more sophisticated method is required for precise quantification of MBF (*2,3,21*). This problem does not seem to have influenced significantly the results of this study, because of the spillover may be similar in the ^{62}Cu-PTSM and $^{13}NH_3$ studies.

CONCLUSION

Copper-62-PTSM is considered to be a promising new PET tracer for evaluating MBF at rest in normal subjects and in patients with CAD as well. The MBF estimates, however, with this agent may be limited in a high flow range.

ACKNOWLEDGMENTS

The authors thank the valuable comments of Drs. Tatsuhiko Hata and Madoka Tateno. Additionally, we thank Hideyuki Taniuchi, BSc, Haruhiro Kitano, BSc, and the Cyclotron staff at Kyoto University Hospital for their technical assistance.

REFERENCES

1. Krivokapich J, Smith GT, Huang SC, et al. Nitrogen-13-ammonia myocardial imaging at rest and with exercise in normal volunteers: quantification of absolute myocardial perfusion with dynamic positron emission tomography. *Circulation* 1989;80:1328–1337.
2. Hutchins GD, Schwaiger M, Rosenspire KC, Krivokapich J, Schelbert HR, Kuhl DE. Noninvasive quantification of regional blood flow in the human heart using ^{13}N-ammonia and dynamic positron emission tomographic imaging. *J Am Coll Cardiol* 1990;15:1032–1042.
3. Krivokapich J, Stevenson LW, Kobashigawa J, Huang SC, Schelbert HR. Quantification of absolute myocardial perfusion at rest and during exercise with positron emission tomography after human cardiac transplantation. *J Am Coll Cardiol* 1991; 18:512–517.
4. Bellina CR, Parodi O, Camici P, et al. Simultaneous in vitro and in vivo validation of nitrogen-13-ammonia for the assessment of regional myocardial blood flow. *J Nucl Med* 1990;31:1335–1343.
5. Choi Y, Huang SC, Hawkins RA, et al. A simplified method for quantification of myocardial blood flow using nitrogen-13-ammonia and dynamic PET. *J Nucl Med* 1993;34:488–497.
6. Bergmann S, Herrero P, Markham J, Weinheimer CJ, Walsh MN. Noninvasive quantitation of myocardial blood flow in human subjects with oxygen-15-labeled water and positron emission tomography. *J Am Coll Cardiol* 1989;14:639–652.
7. Iida H, Kanno I, Takahashi A, et al. Measurement of absolute myocardial blood flow with oxygen-15-water and dynamic positron emission tomography. Strategy for quantification in relation to the partial-volume effect. *Circulation* 1988;78:104–115.
8. Araujo LI, Lammertsma AA, Rhodes CG, et al. Noninvasive quantification of regional myocardial blood flow in coronary artery disease with oxygen-15-labeled carbon dioxide inhalation and positron emission tomography. *Circulation* 1991;83:875–885.
9. Herrero P, Markham J, Shelton ME, Bergmann SR. Implementation and evaluation of a two-compartment model for quantification of myocardial perfusion with rubidium-82 myocardial and positron emission tomography. *Circ Res* 1992;70:496–507.
10. Demer L, Gould K, Goldstein R, et al. Assessment of coronary artery disease severity by positron emission tomography: comparison with quantitative angiography in 193 patients. *Circulation* 1989;79:825–835.
11. Stewert R, Schwaiger M, Molina E, et al. Comparison of rubidium-82 positron emission tomography and thallium-201 SPECT imaging for detection of coronary artery disease. *Am J Cardiol* 1991;67:1303–1310.
12. Go RT, Markwick TH, McIntyre WJ, et al. A prospective comparison of rubidium-82 PET and thallium-201 SPECT myocardial imaging for detection of coronary artery disease. *Am J Cardiol* 1990;31:1899–1905.
13. Schwaiger M. Myocardial perfusion imaging with PET. *J Nucl Med* 1994;35:693–698.
14. Herrero P, Markham J, Shelton ME, Weinheimer CJ, Bergmann SR. Noninvasive quantitation of regional myocardial blood flow with rubidium-82 and positron emission tomography: exploration of a mathematical model. *Circulation* 1990;82: 1377–1386.
15. Green MA. A potential copper radiopharmaceutical for imaging the heart and brain: copper-labeled pyruvaldehyde bis(N4-methylthiosemicarbazone). *Nucl Med Biol* 1987;14:89.
16. Green MA, Klippenstein DL, Tennison JR. Copper(II)bis (thiosemicarbazone) complexes as potential tracers for evaluation of cerebral and myocardial blood flow with PET. *J Nucl Med* 1988;29:1549–1557.
17. Shelton ME, Green MA, Mathias CJ, Welch MJ, Bergmann SR. Kinetics of copper-PTSM in isolated hearts: a novel tracer for measuring blood flow with positron emission tomography. *J Nucl Med* 1989;30:1843–1847.
18. Green MA, Mathias CJ, Welch MJ, et al. Copper-62-labeled pyruvaldehyde *bis*(N^4-methylthiosemicarbazonato)copper(II): synthesis and evaluation as a positron emission tomography tracer for cerebral and myocardial perfusion. *J Nucl Med* 1990;31:1989–1996.
19. Shelton ME, Green MA, Mathias CJ, Welch MJ, Bergmann SR. Assessment of regional myocardial and renal blood flow with copper-PTSM and positron emission tomography. *Circulation* 1990;82:990–997.

20. Beanlands RSB, Music O, Minute M, et al. The kinetics of copper-62-PTSM in the normal human heart. *J Nucl Med* 1992;33:684–690.
21. Herrero P, Markham J, Weinheimer CJ, et al. Quantification of regional myocardial perfusion with generator-produced ^{62}Cu-PTSM and positron emission tomography. *Circulation* 1993;87:173–183.
22. Melon PG, Brihaye C, Degueldre C, et al. Myocardial kinetics of potassium-38 in humans and comparison with copper-62-PTSM. *J Nucl Med* 1994;35:1116–1122.
23. Schwaiger M, Muzik O. Assessment of myocardial perfusion by positron emission tomography. *Am J Cardiol* 1991;67:35D–43D.
24. Fujibayashi Y, Matsumoto K, Yonekura Y, Konishi J, Yokoyama Y. A new zinc-62/copper-62 generator as a copper-62 source for PET radiopharmaceuticals. *J Nucl Med* 1989;30:1838–1842.
25. Petering HG, Buskirk HH, Underwood GE. The antitumor activity of 2-keto-3-ethoxybutylaldehyde bis(thiosemicarbazone) and related compounds. *Cancer Res* 1964;24:367–372.
26. Matsumoto K, Fujibayashi Y, Yonekura Y, et al. Application of the new zinc-62/copper-62 generator: an effective labeling method for ^{62}Cu-PTSM. *Nucl Med Biol* 1992;19:39–44.
27. Tamaki N, Senda M, Yonekura Y, et al. Dynamic positron computed tomography of the heart with a high sensitive positron camera and nitrogen-13-ammonia. *J Nucl Med* 1985;26:567–575.
28. Tamaki N, Yonekura Y, Senda M, et al. Myocardial positron computed tomography with ^{13}N-ammonia at rest and during exercise. *Eur J Nucl Med* 1985;11:246–251.
29. Tamaki N, Yonekura Y, Senda M, et al. Value and limitation of stress thallium-201 single photon emission computed tomography: comparison with nitrogen-13-ammonia positron tomography. *J Nucl Med* 1988;29:1181–1188.
30. Tamaki N, Magata Y, Takahashi N, et al. Oxidative metabolism in the myocardium in normal subjects during dobutamine infusion. *Eur J Nucl Med* 1993;20:231–237.
31. Schelbert HR, Phelps ME, Huang SC, et al. Nitrogen-13-ammonia as an indicator of myocardial blood flow. *Circulation* 1981;61:1259–1272.
32. Klocke FJ. Coronary blood flow in man. *Prog Cardiovasc Dis* 1976;19:117–166.
33. Mathias CJ, Bergmann SR, Green MA. Development and validation of a solvent extraction technique for determination of Cu-PTSM in blood. *Nucl Med Biol* 1993;20:343–349.
34. Okazawa H, Yonekura Y, Fujibayashi Y, et al. Clinical application and quantitative evaluation of generator-produced copper-62-PTSM as a brain perfusion tracer for PET. *J Nucl Med* 1994;35:1910–1915.
35. Rosenspire KC, Schwaiger M, Manger TJ, Hutchins GD, Sutorik A, Kuhle DE. Metabolic fate of [^{13}N]ammonia in humans and canine blood. *J Nucl Med* 1990;31:163–167.
36. Beanlands R, Muzik O, Hutchins GD, et al. Regional tracer distribution of ^{13}N-ammonia and ^{82}Rb in the normal human heart [Abstract]. *Circulation* 1991;84:II-48.
37. Hutchins GD, Beanlands RSB, Muzik O, Schwaiger M. Quantitative versus semi-quantitative PET myocardial blood flow: influence of regional ammonia kinetics. *Circulation* 1992;86:I–710.
38. Porenta G, Czenin J, Huang SC, Kuhle W, Brunken RC, Schelbert HR. Dynamic and gated ^{13}N-ammonia imaging confirms inhomogenous myocardial retention but homogenous perfusion in normal human subjects [Abstract]. *J Nucl Med* 1993;34:35P.
39. Tillisch J, Brunken R, Marshall R, et al. Reversibility of cardiac wall-motion abnormalities predicted by positron tomography. *N Engl J Med* 1986;314:884–888.
40. Tamaki N, Yonekura Y, Yamashita K, et al. Positron emission tomography using fluorine-18 deoxyglucose in evaluation of coronary artery bypass grafting. *Am J Cardiol* 1989;64:860–865.

NUCLEAR CARDIOLOGY

Thallium-201 Reverse Redistribution at Reinjection Imaging Correlated with Coronary Lesion, Wall Motion Abnormality and Tissue Viability

Paolo Marzullo, Alessia Gimelli, Alberto Cuocolo, Leonardo Pace, Claudio Marcassa, Gianmario Sambuceti, Michele Galli, Assuero Giorgetti, Silvia Stefanini, Oberdan Parodi and Antonio L'Abbate

CNR Institute of Clinical Physiology, Pisa, Italy; Nuclear Medicine Department, University Federico II, Napoli, Italy; and Cardiology Division, Fondazione Clinica del Lavoro IRCCS, Veruno, Italy

Previous studies based on standard stress-redistribution ^{201}Tl scintigraphy provided conflicting results about the clinical significance of ^{201}Tl reverse redistribution. Recent observations indicate that the majority of these defects normalize following reinjection reflecting viable myocardium. **Methods:** In this study, the meaning of reverse redistribution occurring at reinjection imaging, its relation to standard 4-hr redistribution, coronary lesion, abnormal wall motion and tissue viability were assessed. A region with normal activity in the stress image was considered as having reverse redistribution if ^{201}Tl activity at reinjection imaging was definitely abnormal with a decrease in relative tracer uptake >15% of the peak. From a series of 270 patients, 29 showed reverse redistribution. Of these 29 patients, 27 had evidence of previous myocardial infarction. Coronary lesions were detected in all but 1 patient. Average ejection fraction was 0.38 ± 0.11. **Results:** On a segmental basis, 50/377 regions showed the pattern of reverse redistribution. A significant coronary lesion (≥50%) was found in 78% of these regions; occlusion rate was 50%, and collateral circulation was found in 35% of occluded vessels. Hypokinesis or akinesis was present in 72% of segments. Tissue viability, defined as an uptake >55% of the peak, was found in 44% of these segments. The 50 segments showing reverse redistribution were divided into two groups according to an abnormal uptake also at 4-hr redistribution (group 1, 25 segments) or appearing only following reinjection (group 2, 25 segments). Despite segments of group 1 showing a higher degree of coronary stenosis (80 ± 32 versus 59 ± 43%, $p < 0.01$), a similar rate of coronary occlusion, ventricular dysfunction and maintained viability was found in the two groups. **Conclusion:** Reverse redistribution in chronic coronary artery disease is frequently associated with significant coronary lesion, collateral-dependent dysfunctioning myocardium and preserved tissue viability. The occurrence of reverse redistribution following reinjection expands the indication for viability imaging to all patients with known coronary artery disease and regional wall motion abnormalities who undergo diagnostic and prognostic ^{201}Tl scintigraphy.

Key Words: thallium-201 scintigraphy; regional ventricular function; coronary artery disease

J Nucl Med 1996; 37:735–741

Clinical studies have demonstrated that the dynamic change in defect extension and severity detected by sequential stress-redistribution ^{201}Tl imaging has a high diagnostic and prognostic accuracy (*1,2*). Furthermore, a series of experimental observations have confirmed these findings in normal, ischemic and hyperemic conditions (*3,4*). The recent introduction of reinjection imaging shifted a great proportion of scintigraphic defects from the fixed to the reversible category, with a reclassification of ^{201}Tl abnormalities (*5,6*).

On the other hand, the observation where initially normal areas of ^{201}Tl uptake subsequently show defects on postexercise images (reverse redistribution) has still neither clinical correlate nor experimental models. Thallium-201 studies performed before the introduction of reinjection imaging provided conflicting results. Some authors showed a good correlation to vessel patency and nontransmural myocardial infarction (*7,8*) that was not observed by others (*9,10*). Technical explanations, such as background oversubtraction or slow redistribution occurring in

Received Mar. 29, 1995; revision accepted Aug. 17, 1995.
For correspondence or reprints contact: Paolo Marzullo, MD, CNR Institute of Clinical Physiology, Via Savi 8, I-56126 Pisa, Italy.